Microsc. Microanal. 16, 755–763, 2010
doi:10.1017/S1431927610093943

Microscopy AND Microanalysis

Unraveling the Role of the *rssC* Gene of *Serratia marcescens* by Atomic Force Microscopy

Bor-Ching Sheu,[1,*] Chih-Chen Lin,[2] Ying-Hsien Fu,[3] Shih-Yuan Lee,[2] Hsin-Chih Lai,[3] Rung-Shin Wu,[2] Chih-Hao Liu,[4] Jui-Chang Tsai,[5] and Shiming Lin[4,5,**]

[1]*Department of Obstetrics and Gynecology, National Taiwan University, Taipei, 100-51, Taiwan*
[2]*Department of Chemistry, Tamkang University, Tamsui, 251-37, Taiwan*
[3]*Department of Medical Biotechnology, Chang Gung University, Tao-Yuan, 333-02, Taiwan*
[4]*Institute of Applied Mechanics, National Taiwan University, Taipei, 106-17, Taiwan*
[5]*Centre for Optoelectronic Biomedicine, National Taiwan University, Taipei, 100-51, Taiwan*

Abstract: The product and direct role of the *rssC* gene of *Serratia marcescens* is unknown. For unraveling the role of the *rssC* gene, atomic force microscopy has been used to identify the surfaces of intact *S. marcescens* wild-type CH-1 cells and *rssC* mutant CH-1ΔC cells. The detailed surface topographies were directly visualized, and quantitative measurements of the physical properties of the membrane structures were provided. CH-1 and CH-1ΔC cells were observed before and after treatment with lysozyme, and their topography-related parameters, e.g., a valley-to-peak distance, mean height, surface roughness, and surface root-mean-square values, were defined and compared. The data obtained suggest that the cellular surface topography of mutant CH-1ΔC becomes rougher and more precipitous than that of wild-type CH-1 cells. Moreover, it was found that, compared with native wild-type CH-1, the cellular surface topography of lysozyme-treated CH-1 was not changed profoundly. The product of the *rssC* gene is thus predicted to be mainly responsible for fatty-acid biosynthesis of the *S. marcescens* outer membrane. This study represents the first direct observation of the structural changes in membranes of bacterial mutant cells and offers a new prospect for predicting gene expression in bacterial cells.

Key words: *Serratia marcescens*, atomic force microscopy (AFM), *rssC* gene, topography

Introduction

Serratia marcescens is a pigmented gram-negative enteric organism (Matsuyama et al., 1989). Unlike most enteric organisms, *S. marcescens* is adapted to a wide variety of ecologic niches. It is found in soil, water, air, plants, and animals (Grimont & Grimont, 1978). In addition, *S. marcescens* is an opportunistic human pathogen that causes many nosocomial infections, particularly in immunocompromised patients and in infants with respiratory ailments (Daschner, 1980). *S. marcescens* CH-1 cells are short rods ($0.5–0.8 \times 1–5\ \mu m^2$) with one to two flagellae in liquid medium. When *S. marcescens* CH-1 are inoculated onto the agar medium surface, they undergo swarming differentiation (Liu et al., 2000).

S. marcescens CH-1ΔC is one mutant of CH-1 that was found to bear a defective *rssC* gene (for repression/regulation of *Serratia* swarming) (Soo et al., 2008), and the gene product was predicted to be involved in cell differentiation, membrane structure construction, and swarming behavior (Liu et al., 2000; Lai et al., 2005). The role of the gene needs to be identified further. Despite the fact that a variety of different methods, such as X-ray crystallography, neutron diffraction, and mass spectrometry, has been used to study the role of an unknown gene involved in membrane construction, relatively little work has been applied to identification of a gene by directly observing the structural changes in membranes (Ibrahim et al., 2009). It is worth observing the cell-surface topography change in mutant *S. marcescens* CH-1ΔC in more detail by use of atomic force microscopy (AFM).

Atomic force microscopy, a nanoresolution technique that needs no complex preparation procedure for the biological sample (Binnig et al., 1986), has proved over the past few years to be a suitable approach for imaging and identifying single molecules (Wacker et al., 2007; Chernov et al., 2008; Neaves et al., 2009) and native biological membranes (Matyka et al., 2007; Olsen et al., 2008; Wang et al., 2009). Three-dimensional (3D) information can be extracted directly from AFM topographic and phase images. Topographic images of either intact or isolated membranes of

Received March 17, 2010; accepted August 10, 2010
**Corresponding author*. E-mail: bcsheu@ntu.edu.tw
***Corresponding author*. E-mail: til@ntu.edu.tw

bacterial cells have been published (Cross et al., 2007; Mohanty & Berry, 2008; Dupres et al., 2009) and have revealed structural details that could not be detected by other approaches. These advantages caused us to apply AFM to the field of membrane structure and analysis of gene expression.

In this study, we demonstrated that AFM can be employed for investigating the membrane construction of *S. marcescens* CH-1ΔC so that we could unravel the role of the *rssC* gene. In concordance with the AFM observation, surface features were further investigated with transmission electron microscopy (TEM). Also, the total cellular fatty-acid profiles were determined by gas-chromatography analysis. This study represents the first direct characterization of the *rssC* gene by measurement of structural changes in membranes of intact *S. marcescens* cells on a nanometer scale.

Materials and Methods

S. marcescens CH-1 and CH-1ΔC Preparation

S. marcescens wild-type CH-1 and mutant CH-1ΔC cells were cultured overnight on LB (L3022, Sigma Chemical Company, NY, USA) medium. The bacterial culture was then diluted 1:100 with fresh LB broth and incubated at 37°C with vigorous shaking (225 rpm) for 2 h. Prior to imaging, bacterial cultures were centrifuged at 2,050 *g* for 5 min at 4°C. The wet pellet was resuspended in distilled water, recentrifuged (2×) to remove the growth medium, and the final pellet was again suspended in distilled water for attachment to poly-L-lysine-treated mica.

Lysozyme Treatment

Lysozyme from chicken egg white (95% Grade-I, Sigma Chemical Company, NY; 0.91 mg) was dissolved in 1.5 mL of 0.2 M HEPES buffer, pH 7.5. A 20 μL portion of the above lysozyme solution (50,000 units/mL) was added to 1.0 mL of the *S. marcescens* CH-1 and CH-1ΔC suspension. The mixture was incubated for 5 min at room temperature, followed by an additional 5 min at 4°C. The suspension was centrifuged at 2,050 *g* for 5 min, and the pellet was washed and resuspended in water (250 μL) for analysis. A final concentration of about 10^4–10^5 cells/mL was used for attachment to poly-L-lysine-treated mica.

Protease Treatment

Protease from *Streptomyces griseus* (P5147, Sigma, USA) was dissolved in 10 mM sodium acetate buffer with 5 mM calcium acetate, pH 7.5, at a concentration of 1 mg/mL (stock solution). A 50 μL portion of the above protease solution (20 units/mL) was added to 1.0 mL of aqueous *S. marcescens* CH-1 and CH-1ΔC suspension (approximately 7.5×10^7 cells). The mixture was incubated at 37°C for 20 min. *S. marcescens* cells were then pelleted by centrifugation at 2,050 *g* for 5 min, resuspended in distilled water, and recentrifuged (2×). The final pellet was again suspended in distilled water (1 mL) prior to attachment to poly-L-lysine-treated mica.

Attachment of Bacteria to Poly-L-Lysine-Treated Mica

For AFM studies, *S. marcescens* CH-1 or CH-1ΔC cells were attached through electrostatic interactions (physical adsorption) by placement in contact with a glass slide that had been coated with poly-L-lysine hydrobromide, a positively charged compound. After cleaning of the slide with methanol and Milli-Q water, a drop of 0.01% (wt/vol) poly-L-lysine hydrobromide solution was added and incubated for 30 min. The slide surface was then washed with Milli-Q water before introduction of the bacteria. The surface was then washed with distilled water (50 μL, 3×) and allowed to dry in air.

AFM Analysis

The AFM experiments under a tapping mode of operation were carried out with a Smena B™ AFM (NT-MDT Co., Moscow). Commercial silicon cantilevers Ultrasharp™ NSG11 (NT-MDT Co., Moscow) with a spring constant of 0.06 N/m was used for the tapping mode. We collected the images in a narrow range of frequencies, ranging from 120–130 kHz. The oscillation amplitude was 50–100 nm, with a setpoint ratio of 0.9. Light tapping was used, which involved maintaining a high amplitude setpoint relative to the free amplitude of the cantilever. Typically, we began by scanning a 10×10 μm^2 area that contained several bacterial cells. Gradually, the image size was reduced to a few isolated cells. These bacteria cells were then scanned in both directions several times before an image was captured, to help ensure that tip artifacts, such as hysteresis, were not altering the images. For each preparation, we then selected at least three and up to six high-quality images to be captured. One image of the selection was chosen for the 3D presentation. Tips were replaced frequently, or when there was an indication of artifacts present in the images. After the images were recorded, an offline section analysis was performed on each image to gain information on the sample topography. A "valley to peak" value ($R_{\max}$) defines the difference between the maximum and minimum values of the z coordinate on the surface within the analysis area (height drop): $R_{\max} = z_{\max} - z_{\min}$. A "mean height" value (R_{mean}) defines the z-coordinate average value on the sample surface within the analysis area:

$$R_{mean} = Z_{mean} = \frac{1}{N_x N_y} \sum_{i=1}^{N_x} \sum_{j=1}^{N_y} Z_{ij}, \quad z = z_{ij} - R_{mean}.$$

A "surface roughness" value (R_a) analysis was also performed on each sample, which defines the average value of the surface roughness within the area being analyzed:

$$R_a = \frac{1}{N_x N_y} \sum_{i=1}^{N_x} \sum_{j=1}^{N_y} z|(i,j) - z_{mean}|,$$

$$Z_{mean} = \frac{1}{N_x N_y} \sum_{i=1}^{N_x} \sum_{j=1}^{N_y} Z_{ij}.$$

The surface "root-mean-square" value (R_q) was calculated as the standard deviation for the z coordinate on the sample surface within the area being analyzed:

$$R_q = \sqrt{\frac{1}{N_x N_y} \sum_{i=1}^{N_x} \sum_{j=1}^{N_y} (z(i,j) - z_{mean})^2}.$$

Statistical Analysis

All measurements over the AFM images were performed in triplicate and pooled results of independent experiments with a total of 24 individual targets were analyzed. Data were expressed as mean ± standard error (SE) unless otherwise indicated. One-way ANOVA was first performed among variables, and then the paired-samples T test was utilized to confirm the possible significant difference. A generalized estimation equation for correlated data of repeated measurements was used to compare parameters of mean height distribution curves over the AFM images. Statistical significance was defined by a P value less than 0.05.

TEM Analysis

Cells were observed in TEM using a HITACHI H-7100 TEM operated at 50 kV with the cold trap in place. For TEM analysis, bacteria were adsorbed to 200 mesh copper electron microscopy grids coated with carbon and Formvar. The grids were then floated on a drop of 1% (wt/vol) phosphotungstic acid for 15 s for negative staining of the sample.

Gas Chromatography

Strains were incubated in LB broth medium at 37°C overnight. After overnight culture, bacteria were seeded on an LB plate for 2 h. Samples were prepared for use in gas chromotography (GC)-FAME analysis (Microbe Inotech Laboratories, Inc., St. Louis, MO, USA).

Statistical Analysis

All analyses in the acyl chain composition by GC were performed in three independent experiments with triplicate measurements and pooled results of independent experiments with a total of nine individual targets were analyzed. Data were expressed as mean ± SE unless otherwise indicated. One-way ANOVA was first performed among variables and then the paired-samples T test was utilized to confirm the possible significant difference. A generalized estimation equation for correlated data of repeated measurements was used to compare parameters of mean acyl chain composition. Statistical significance was defined by a P value less than 0.05.

Results and Discussion

GenBank Database Search of *rssC* Gene

A search of the GenBank database with the amino-acid sequence of the *rssC* gene was performed, and the sequence was shown to be highly homologous to members of the integral membrane transacylase protein family, whose function is related to lipid biosynthesis (data not shown). The function of transacylase or acyltransferase is to transfer the acyl chain (including the acetyl chain) from its respected acyl carrier protein to the target substrate, either glycerol or polysaccharide and even acyl chains, and is related to lipid metabolism. As a result, this enzyme may be connected to fatty-acid biosynthesis or modification of the cell membrane component, such as PlsB, PlsC, LpxA, LpxD, LpxL, LpxM, whose functions are related to (a) lipopolysaccharide (LPS) biosynthesis and (b) phospholipid biosynthesis as in *Escherichia coli* and *Salmonella typhimurium* (Raetz & Whitfield, 2002; Rock & Jackowski, 2002). Thus, the *rssC* gene is predicted to be an acyl transferase and to be mainly responsible for the acylation of either LPS modification (O-chain acetyl transferase) or fatty-acid biosynthesis of the outer and inner leaflets (acyl transferase) on *S. marcescens* cells (Fig. 1).

AFM Analysis of Native CH-1 and CH-1ΔC

For studying the role of the *rssC* gene of *S. marcescens* in membrane construction, AFM was used to observe and identify the surface structures of wild-type CH-1 and mutant CH-1ΔC cells in more detail. The detailed cellular surface topographies of CH-1 and CH-1ΔC were studied by use of AFM by systematically zooming in on desired cells and regions within the cell membrane (Fig. 2). A larger scan area ($10 \times 10\ \mu m^2$) was first made for wild-type CH-1 (Fig. 2A) and *rssC* mutant CH-1ΔC cells (Fig. 2B) to select the cells desired for higher-resolution images. As shown in Figures 2A and 2B, CH-1 and CH-1ΔC cells are readily distinguishable. An image of an individual rod-shaped cell acquired by zooming into the boxed area of Figures 2A and 2B is shown in Figures 2A′ and 2B′, respectively.

It is reported that the differentiation markers, including cell division and cell elongation, were controlled by *flhDC* in *S. marcescens* (Liu et al., 2000). To see whether the cell elongation pattern was aberrant, following the growth, the cell length of CH-1 and CH-1ΔC were measured from Figures 2A and 2B. Quantitative measurements of the dimensions of the cells were made and revealed that the measured lengths of CH-1 and CH-1ΔC were approximately 2108 nm and 1996 nm, respectively. More than 20 cells were then

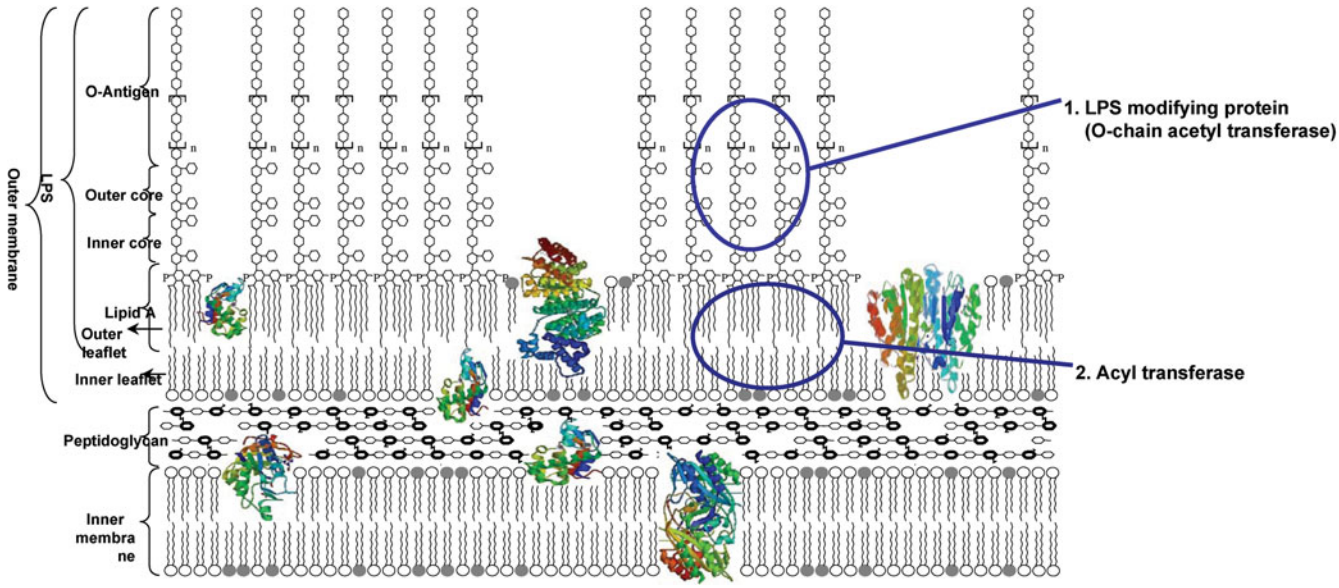

Figure 1. The gram-negative bacterial *S. marcescens* envelope consists of two lipid bilayers (inner or cytoplasmic membrane and outer membrane) composition that are separated by the soluble periplasmic space. The *rssC* gene is predicted to be an acyl transferase and to be mainly responsible for the acylation of either LPS modification (O-chain acetyl transferase) or fatty-acid biosynthesis in the outer and inner leaflets (acyl transferase) of *S. marcescens*.

randomly chosen under AFM imaging, and lengths were measured. The average length of CH-1 is 2,282.30 ± 187.22 nm, and that of CH-1ΔC is 2,005.64 ± 194.51 nm. The cell length of CH-1ΔC was consistently observed to be shorter than CH-1 ($n = 24$, $P < 0.01$ by paired-samples T test). The data were further confirmed by light-microscopic observation (data not shown). The data indicated that the cell differentiation process was affected in *rssC* mutant CH-1ΔC, possibly through the flagellar *flhDC* master operon (Liu et al., 2000).

Higher-resolution images acquired by zooming into the boxed areas of Figures 2A′ and 2B′ are displayed in Figures 2A″ and 2B″, respectively. As shown in Figures 2A″ and 2B″, the exemplary AFM images showed that many protrusions shaped like mountain ranges and hills exist on the wild-type CH-1 and mutant CH-1ΔC surfaces, respectively. Data of the mean height distribution curves over the AFM images were analyzed by a generalized estimation equation for correlated data of repeated measurements and shown in Figures 2a and 2b, respectively. The protrusions are likely to be LPS and proteins such as porin proteins, lipoproteins, matrix proteins, and high-affinity receptors located on the outer membrane of *S. marcescens* CH-1 and CH-1ΔC, as depicted in the models of the cell wall (Fig. 1), and as shown by Ehrenhofer et al. (1997) and Matsuyama et al. (1995).

To investigate the detailed surface feature further, we then examined more than 20 individual CH-1 and CH-1ΔC cells with AFM. Statistical analysis with ANOVA was first performed among variables and then a paired-samples T test was utilized to confirm the possible significant difference on the AFM images. The data are summarized in Table 1A,B. We found that, compared with wild-type CH-1 (Table 1A), the cellular surface topography of *rssC* mutant CH-1ΔC (Table 1B) was indeed changed. The data suggest that the surface structure of *rssC* mutant CH-1ΔC becomes more precipitous (R_{max} increase by 39.09%) and rougher (R_a increase by 53.23%) than that of wild-type CH-1 cells, as indicted in Table 1E. In explanation of the data presented above, cell wall modes were made and contour views from within the membrane with the extracellular region above and the intracellular region below are depicted in Figure 3A (for a wild-type CH-1 cell) and Figure 3B (for an *rssC* mutant CH-1ΔC cell), respectively. In Figure 3B, the cell membrane aberrance sites (as indicated by the red circles) are located in the LPS layer or both outer and inner leaflets of mutant CH-1ΔC cells.

AFM Analysis of Lysozyme-Treated CH-1 and CH-1ΔC

In addition, it was suggested that cell membrane aberrance in *rssC* mutant CH-1ΔC might allow the lysozyme to penetrate and digest the peptidoglycan layer (Camesano et al., 2000). CH-1 and CH-1ΔC cells treated with lysozyme were imaged and are shown in Figures 2C and 2D, respectively. As shown in Figures 2C″ and 2D″, the AFM images showed that many protrusions shaped like mountain ranges and hills exist on the lysozyme-treated CH-1 (Fig. 2C″) and CH-1ΔC (Fig. 2D″) cell surfaces, respectively. Data of the mean height distribution curves over the AFM images were

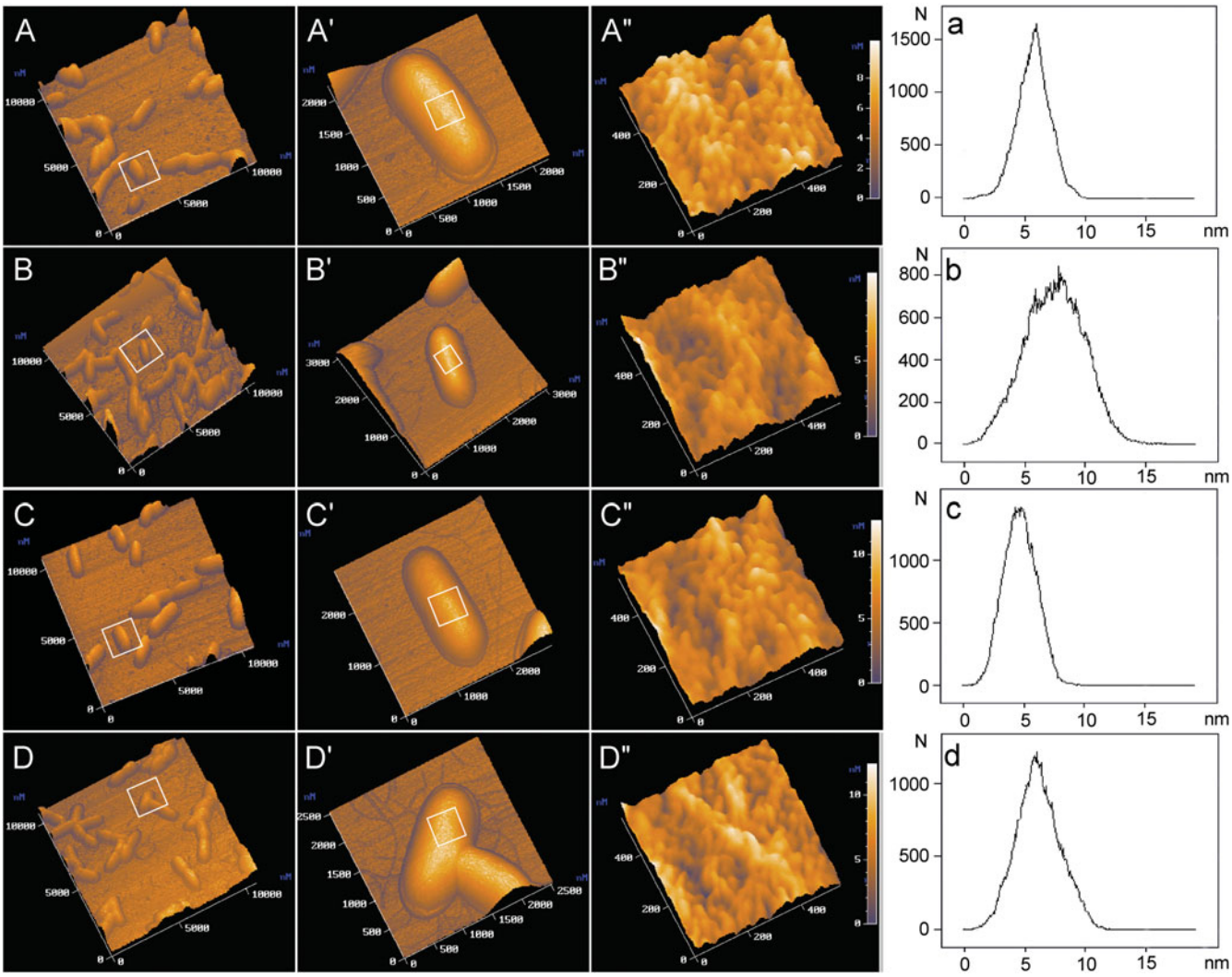

Figure 2. Three-dimensional AFM topographic images of (**A**) wild-type CH-1 and (**B**) *rssC* mutant CH-1ΔC of native *S. marcescens* cells. Three-dimensional AFM topographic images of (**C**) wild-type CH-1 and (**D**) *rssC* mutant CH-1ΔC of *S. marcescens* cells after treatment with lysozyme. Images acquired by zooming into the boxed areas of the first column are displayed in the second column. Images acquired by zooming into the boxed areas of the second column are displayed in the third column. The AFM scanning areas are 10×10 (the first column), 3×3 (the second column), and 0.5×0.5 (the third column) μm^2 for the low- and higher-resolution images, respectively. The *y*-axis represents the height of features (nm). (**a–d**) Statistical analysis (mean height distribution curve) were performed over the AFM images and displayed in the fourth column.

analyzed by a generalized estimation equation for correlated data of repeated measurements and shown in Figures 2c and 2d, respectively. More than 20 individual CH-1 and CH-1ΔC cells after treatment with lysozyme were then examined. Data on the AFM image and the topographic parameters are summarized in Table 1C,D. It was found that, compared with native wild-type CH-1 (Table 1A), the cellular surface topography of wild-type CH-1 showed a mean decrease of 5.48% in R_{max}, 5.82% in R_{mean}, 6.45% in R_a, and 7.14% in R_q after lysozyme-treatment (Table 1F). On the contrary, the cellular surface topography of lysozyme-treated *rssC* mutant CH-1ΔC (Table 1D) was obviously changed, with a mean decrease of 22.52% in R_{max}, 13.47% in R_{mean}, 26.84% in R_a, and 25.21% in R_q (Table 1G). Statistically significant differences existed when we compared all the cellular surface parameters between the lysozyme-treated/untreated native wild-type and mutant CH-1ΔC (Table 1F,G, $P < 0.05$).

Based on the data presented above, we propose the following models for the cell wall structure (Fig. 3). As depicted in Figure 3A,C, the peptidoglycan layer between the outer and inner membrane of wild-type CH-1 was slightly changed after treatment with lysozyme, which implies that lysozyme minimally penetrates the outer mem-

Table 1. Data with Statistical Analyses of Cellular Surface Topographies of *rssC* Mutant CH-1ΔC Compared with Wild-Type CH-1 Before and After Treatment with Lysozyme.*

	(A) Wild-Type CH-1 ($n = 24$) (nm)	(B) Mutant CH-1ΔC ($n = 24$) (nm)	(C) Lysozyme-Treated CH-1 ($n = 24$) (nm)	(D) Lysozyme-Treated CH-1ΔC ($n = 24$) (nm)	(E) = [(B) − (A)]/(A) (%)	(F) = [(A) − (C)]/(A) (%)	(G) = [(B) − (D)]/(B) (%)
Valley to peak (R_{max})	10.95 ± 1.04[a]	15.23 ± 1.34[a]	10.35 ± 1.91	11.80 ± 2.49	39.09	5.48[b]	22.52[b]
Mean height (R_{mean})	5.50 ± 0.39[a]	6.98 ± 0.38[a]	5.18 ± 0.68	6.04 ± 0.82	26.91	5.82[b]	13.47[b]
Surface roughness (R_a)	1.24 ± 0.18[a]	1.90 ± 0.20[a]	1.16 ± 0.16	1.39 ± 0.30	53.23	6.45[b]	26.84[b]
Root-mean-square (R_q)	1.54 ± 0.20[a]	2.34 ± 0.85[a]	1.43 ± 0.32	1.75 ± 0.22	51.95	7.14[b]	25.21[b]

*Data are expressed as mean ± *SE* (A)–(D) or percentage of decrease (E)–(G).
[a] $P < 0.05$ by ANOVA and paired sample T test when comparing wild-type CH-1 with mutant CH-1ΔC.
[b] $P < 0.05$ by generalized estimation equation for correlated data of repeated measurements when comparing the lysozyme-induced percentage of decrease between wild-type CH-1 and mutant CH-1ΔC.

brane layer and digests the peptidoglycan layer of wild-type CH-1 cells. Contrarily, as depicted in Figure 3B,D, the peptidoglycan layer between the outer and inner membrane of wild-type CH-1 was obviously changed after treatment with lysozyme, which indicated that lysozyme can penetrate the outer membrane layer and directly digest the peptidoglycan layer of mutant CH-1ΔC cells. Our findings illustrated that certain parts of the mutant CH-1ΔC cell membrane were more seriously collapsed by lysozyme, and resulted in far less roughness (decrease R_a) and a flattened surface (decrease of R_{max}) (Table 1F,G).

Accordingly, our data indicate that mutation in the *rssC* gene does alter the outer membrane structure of *S. marcescens* wild-type CH-1 cells. The *rssC* gene is thus predicted to be mainly responsible for the acylation of either LPS modification or fatty-acid biosynthesis of the outer and inner leaflets on *S. marcescens* cells. In addition, it was found that the data were basically consistent with TEM observation and cellular fatty acid profile analysis.

TEM Analysis

Because the *rssC* gene is predicted to be involved in membrane construction, it is worthwhile to observe the cell surface structures of wild-type CH-1 and mutant CH-1ΔC in more detail by TEM. TEM images showed that there was a light marginal ring suggested to be either a capsule or LPS around the wild-type cell (Fig. 4A), whereas mutant cells (Fig. 4B) seemed to be aberrant and had small blebs (white arrows). The results indicated that a defect in the *rssC* gene altered the bacterial cell membrane structure.

Mutation in the *rssc* Gene Alters the Cellular Fatty-Acid Profile

In concordance with the results observed by AFM, total cellular fatty acids were further analyzed by gas chromatography. The *rssC* gene is expected to be an acyl transferase. Therefore, a defect in this protein might result in alteration of the fatty-acid composition. After extraction, the total cellular fatty acid profile of CH-1 and CH-1ΔC was determined by gas chromatography. The data obtained from three independent experiments with triplicate measurements (Fig. 5) showed that the acyl chain composition in CH-1 was different from that in CH-1ΔC, especially the short chain C12:0 (6.2% versus 3.1%, $n = 9$, $P < 0.01$), branched chains C15:0 anteiso (3.3% versus 2.5%, $n = 9$, $P < 0.05$) and C14:0 OH (0.1% versus 2.3%, $n = 9$, $P < 0.01$) but not C18:0 (2.4% versus 2.1%, $n = 9$, $P = 0.057$). These results indicated that mutation in the *rssC* gene has altered the cellular fatty acid composition.

Kloser et al. (1998) showed that modulation of the ratio between lipid A and phospholipid components might influence outer-membrane protein assembly. The distinction of cell surface topographies between wild-type CH-1 and mutant CH-1ΔC as revealed by AFM might occur indirectly.

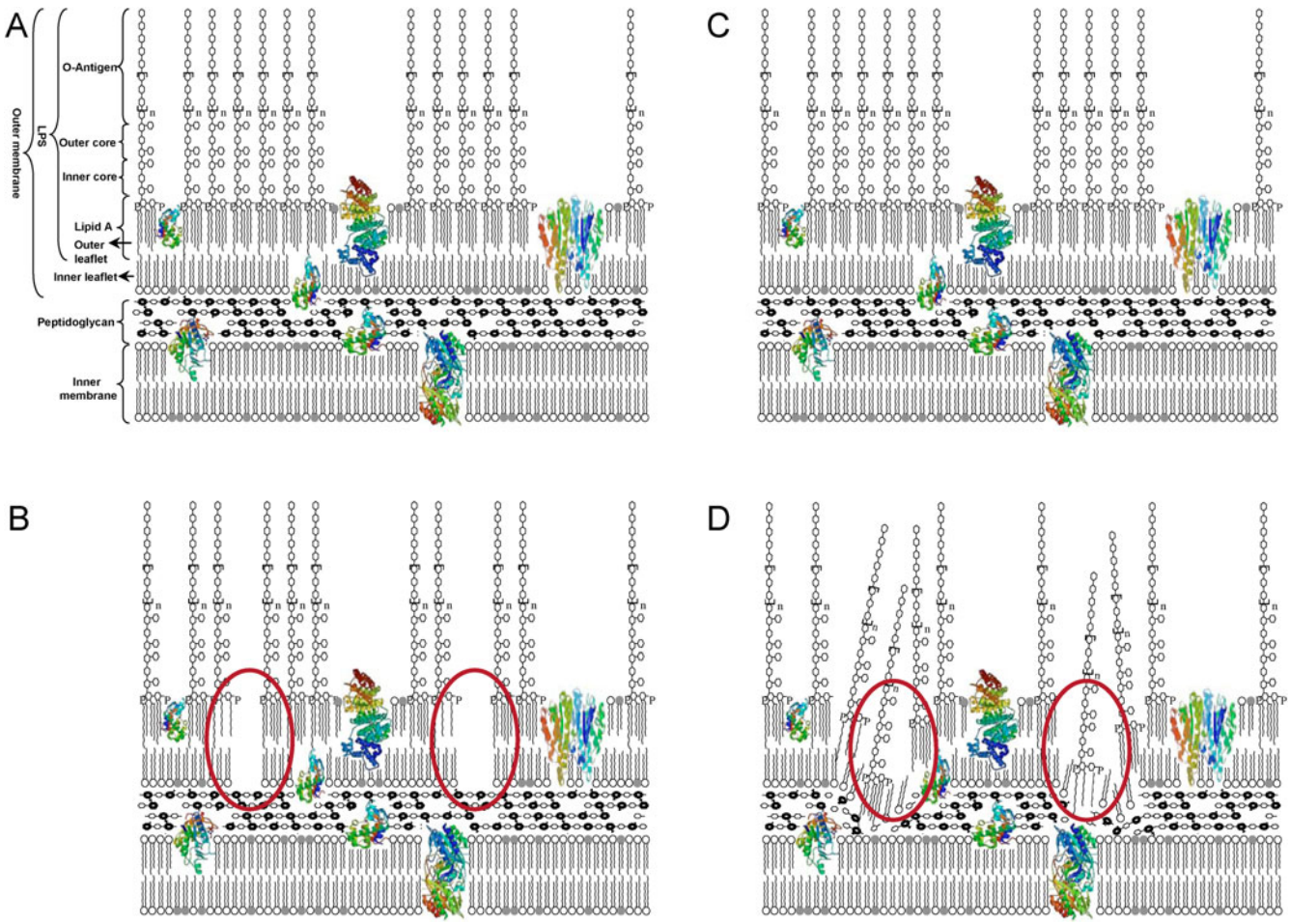

Figure 3. (Color online) Cell wall models of wild-type *S. marcescens* CH-1 and *rssC* mutant CH-1ΔC before and after treatment with lysozyme. Four contour views from within the membrane with the extracellular region above and the intracellular region below are displayed in (**A**) for wild-type CH-1, (**B**) for *rssC* mutant CH-1ΔC, (**C**) for wild-type CH-1 after treatment with lysozyme, and (**D**) for mutant CH-1ΔC after treatment with lysozyme. In **B** and **D**, the cell membrane aberrance sites (as indicated by the red circles) are located in the LPS layer or both outer and inner leaflets of mutant CH-1ΔC cells.

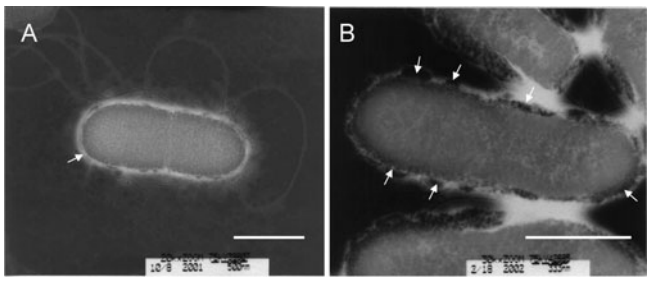

Figure 4. Electron micrographs of *S. marcescens*. TEM images of (**A**) wild-type CH-1 and (**B**) mutant CH-1ΔC. Bar: 1 μm. Images showed that there was a light marginal ring suggested to be either a capsule or LPS around the wild-type CH-1 cell, whereas the mutant CH-1ΔC cell seemed to be aberrant and small blebs were present (white arrows).

First, a defect in the *rssC* gene resulted in the alteration of fatty-acid biosynthesis, even though the genes related to LPS or membrane biosynthesis worked normally. Then, the complete structure of the cell-wall-associated LPS or even the peptidoglycan layer is disrupted, leading to abnormal cell membrane protein assembly. Finally, an aberrant cell wall was also observed in CH-1ΔC under TEM observation.

Conclusions

We have shown that AFM is a useful technique in providing quantitative measurements of the physical properties of the

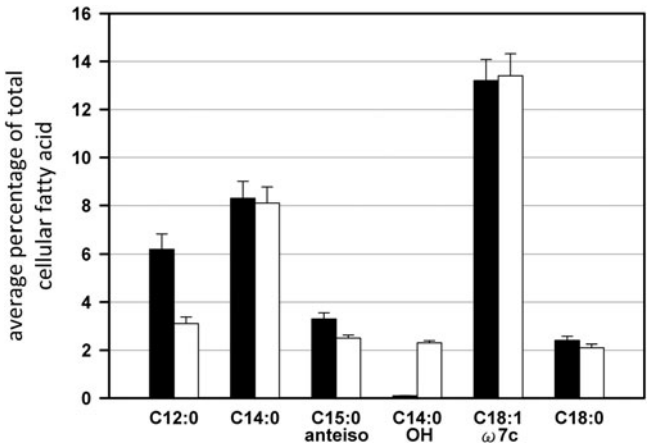

Figure 5. Gas-chromatography analysis of total cellular fatty acids between wild-type CH-1 (white bars) and *rssC* mutant CH-1ΔC (black bars) cells. The data were obtained from three independent experiments with triplicate measurements. [C12:0] is *n*-dodecanoic acid; [C14:0] is *n*-tetradecanoic acid; [C15:0 anteiso] is anteiso-3-methyl-tetradecanoic acid; [C14:0 OH] is 2-hydroxyl-tetradecanoic acid; [C18:1 *ω*7c] is *cis*-9-octadecenoic acid, and [C18:0] is *n*-9-octadecanoic acid.

membrane structures for individual intact *S. marcescens* wild-type CH-1 or *rssC* mutant CH-1ΔC cells. In addition, 3D information on surface features in the membrane of CH-1 and CH-1ΔC cells can be extracted from the topographic images before and after treatment with lysozyme, and their topography-related parameters can be defined and compared. The results obtained from physical measurements of CH-1 and CH-1ΔC cells before and after treatment by AFM may suggest that mutation in the *rssC* gene does alter the outer membrane structure of *S. marcescens*. Moreover, it was found that the AFM data were consistent with the TEM observation and cellular fatty acid profile analysis. Taken together, the *rssC* gene is predicted to be mainly responsible for fatty-acid biosynthesis of the *S. marcescens* outer membrane, and the cell membrane aberrance sites are assumed to be located in the lipid A layer or the inner leaflet in mutant CH-1ΔC. We have presented a way to examine the role of the *rssC* gene of *S. marcescens*. It allows the direct observation of structural changes in membranes of bacterial mutant cells and possible prediction of gene function in bacterial cells.

Acknowledgments

This study was supported by grants from the National Science Council (NSC96-2221-E-002-257-MY3, NSC98-2314-B-002-099MY3, NSC98-2320-B-002-006-MY3, NSC98-3114-B-002-001).

References

Binnig, G., Quate, C.F. & Gerber, C. (1986). Atomic force microscope. *Phys Rev Lett* **56**, 930–933.

Camesano, T.A., Natan, M.J. & Logan, B.E. (2000). Observation of changes in bacterial cell morphology using tapping mode atomic force microscopy. *Langmuir* **16**, 4563–4572.

Chernov, K.G., Curmi, P.A., Hamon, L., Mechulam, A., Ovchinnikov, L.P. & Pastre, D. (2008). Atomic force microscopy reveals binding of mRNA to microtubules mediated by two major mRNP proteins YB-1 and PABP. *FEBS Lett* **582**, 2875–2881.

Cross, S.E., Kreth, J., Zhu, L., Sullivan, R., Shi, W.Y., Qi, F.X. & Gimzewski, J.K. (2007). Nanomechanical properties of glucans and associated cell-surface adhesion of Streptococcus mutans probed by atomic force microscopy under *in situ* conditions. *Microbiology-Sgm* **153**, 3124–3132.

Daschner, F.D. (1980). The epidemiology of *Serratia marcescens*. In *The Genus Serratia*, Graevenitz, A. & Rubin, S.J. (Eds.), pp. 187–196. Boca Raton, FL: CRC Press.

Dupres, V., Alsteens, D., Pauwels, K. & Dufrene, Y.F. (2009). *In vivo* imaging of S-layer nanoarrays on *Corynebacterium glutamicum*. *Langmuir* **25**, 9653–9655.

Ehrenhofer, U., Rakowska, A., Schneider, S.W., Schwab, A. & Oberleithner, H. (1997). The atomic force microscope detects ATP-sensitive protein clusters in the plasma membrane of transformed MDCK cells. *Cell Biol Int* **21**, 737–746.

Grimont, P.A.D. & Grimont, F. (1978). Genus Serratia. *Ann Rev Microbiol* **32**, 221–248.

Ibrahim, K.S., Bakkiyaraj, D., James, R., Babu, T.G. & Pandian, S.T.K. (2009). Isolation and sequence analysis of a small cryptic plasmid pRK10 from a corrosion inhibitor degrading strain *Serratia marcescens* ACE2. *Plasmid* **62**, 183–190.

Kloser, A., Laird, M., Deng, M. & Misra, R. (1998). Modulations in lipid A and phospholipid biosynthesis pathways influence outer membrane protein assembly in *Escherichia coli* K-12. *Molec Microbiol* **27**, 1003–1008.

Lai, H.C., Soo, P.C., Wei, J.R., Yi, W.C., Liaw, S.J., Horng, Y.T., Lin, S.M., Ho, S.W., Swift, S. & Williams, P. (2005). The RssAB two-component signal transduction system in *Serratia marcescens* regulates swarming motility and cell envelope architecture in response to exogenous saturated fatty acids. *J Bacteriol* **187**, 3407–3414.

Liu, J.H., Lai, M.J., Ang, S., Shu, J.W., Soo, P.C., Horng, Y.T., Yi, W.C., Lai, H.C., Luh, K.T., Ho, S.W. & Swift, S. (2000). Role of flhDC in the expression of the nuclease gene nucA, cell division and flagellar synthesis in *Serratia marcescens*. *J Biomed Sci* **7**, 475–483.

Matsuyama, T., Bhasin, A. & Harshey, R.M. (1995). Mutational analysis of flagellum-independent surface spreading of *Serratia marcescens*-274 on a low-agar medium. *J Bacteriol* **177**, 987–991.

Matsuyama, T., Sogawa, M. & Nakagawa, Y. (1989). Fractal spreading growth of *Serratia marcescens* which produces surface-active exolipids. *Fems Microbiol Lett* **61**, 243–246.

Matyka, K., Matyka, M., Mroz, I., Zalewska-Rejdak, J. & Ciszewski, A. (2007). An AFM study on mechanical properties of native and dimethyl suberimidate cross-linked pericardium tissue. *J Mol Recognition* **20**(6), 524–530.

Mohanty, N. & Berry, V. (2008). Graphene-based single-bacterium resolution biodevice and DNA transistor: Interfacing graphene

derivatives with nanoscale and microscale biocomponents. *Nano Lett* **8**, 4469–4476.

Neaves, K.J., Huppert, J.L., Henderson, R.M. & Edwardson, J.M. (2009). Direct visualization of G-quadruplexes in DNA using atomic force microscopy. *Nucl Acids Res* **37**, 6269–6275.

Olsen, J.D., Tucker, J.D., Timney, J.A., Qian, P., Vassilev, C. & Hunter, C.N. (2008). The organization of LH2 complexes in membranes from *Rhodobacter sphaeroides*. *J Biol Chem* **283**, 30772–30779.

Raetz, C.R.H. & Whitfield, C. (2002). Lipopolysaccharide endotoxins. *Ann Rev Biochem* **71**, 635–700.

Rock, C.O. & Jackowski, S. (2002). Forty years of bacterial fatty acid synthesis. *Biochem Biophys Res Comm* **292**, 1155–1166.

Soo, P.C., Horng, Y.T., Fu, Y.H., Lu, C.C. & Lai, H.C. (2008). A potential acyltransferase regulates swarming in *Serratia marcescens*. *Biochem Biophys Res Comm* **371**, 462–467.

Wacker, D.A., Ruhl, D.D., Balagamwala, E.H., Hope, K.M., Zhang, T. & Kraus, W.L. (2007). The DNA binding and catalytic domains of poly(ADP-ribose) polymerase I cooperate in the regulation of chromatin structure and transcription. *Mol Cell Biol* **27**, 7475–7485.

Wang, J., Wan, Z., Liu, W., Li, L., Ren, L., Wang, X., Sun, P., Ren, L., Zhao, H., Tu, Q., Zhang, Z., Song, N. & Zhang, L. (2009). Atomic force microscope study of tumor cell membranes following treatment with anti-cancer drugs. *Biosens Bioelectron* **25**, 721–727.